

ORBITAL EVOLUTION OF COMPACT WHITE DWARF BINARIES

DAVID L. KAPLAN¹, LARS BILDSTEN^{2,3}, & JUSTIN D. R. STEINFADT³

ApJ, in press

ABSTRACT

The new-found prevalence of extremely low mass (ELM, $M_{\text{He}} < 0.2 M_{\odot}$) helium white dwarfs (WDs) in tight binaries with more massive WDs has raised our interest in understanding the nature of their mass transfer. Possessing small ($M_{\text{env}} \sim 10^{-3} M_{\odot}$) but thick hydrogen envelopes, these objects have larger radii than cold WDs and so initiate mass transfer of H-rich material at orbital periods of 6–10 minutes. Building on the original work of D’Antona et al., we confirm the 10^6 yr period of continued inspiral with mass transfer of H-rich matter and highlight that the inspiraling direct-impact double WD binary HM Cancri likely has an ELM WD donor. The ELM WDs have less of a radius expansion under mass loss, thus enabling a larger range of donor masses that can stably transfer matter and become a He mass transferring AM CVn binary. Even once in the long-lived AM CVn mass transferring stage, these He WDs have larger radii due to their higher entropy from the prolonged H burning stage.

Subject headings: nuclear reactions, nucleosynthesis, abundances — supernovae: Type Ia — white dwarfs

1. INTRODUCTION

Helium core white dwarfs (WDs) are made from $< 2.0 M_{\odot}$ stars when stellar evolution is truncated before the He core reaches the $M_{\text{He}} \approx 0.48 M_{\odot}$ needed for the helium core flash. One formation mechanism is significant mass loss due to stellar winds on the red giant branch (RGB) that strips the H envelope (D’Cruz et al. 1996), typically leading to $M_{\text{He}} = 0.4 - 0.48 M_{\odot}$ (Hansen 2005; Kalirai et al. 2007; Kilic, Stanek, & Pinsonneault 2007b). Another mechanism is a common envelope induced by binary interactions (Iben & Livio 1993; Marsh, Dhillon, & Duck 1995), making extremely low-mass (ELM) He WDs ($M_{\text{He}} < 0.20 M_{\odot}$ or so) when the interaction occurs at the base of the RGB (see van Kerkwijk, Bergeron, & Kulkarni 1996). These ELM He WDs were first seen as companions to millisecond pulsars (e.g., Bassa et al. 2006) or in high proper motion catalogs (Kawka et al. 2006; Kawka & Vennes 2009), but the advent of the Sloan Digital Sky Survey (Eisenstein et al. 2006) and other surveys revealed many additional ELM WDs (Kilic et al. 2007b; Badenes et al. 2009; Mullally et al. 2009; Kilic et al. 2010b; Marsh et al. 2011; Kulkarni & van Kerkwijk 2010; Steinfadt et al. 2010b; Kilic et al. 2011c,a; Parsons et al. 2011; Marsh 2011; Brown et al. 2011b; Kilic et al. 2011b; Vennes et al. 2011; Kilic et al. 2012, and Figure 1).

ELM WDs were predicted to possess stably burning H envelopes ($M_{\text{env}} \sim 10^{-3} - 10^{-2} M_{\odot}$) that keep them bright for Gyrs (Serenelli et al. 2002; Panei et al. 2007), and this has certainly aided the recent detections (Kilic et al. 2011a; Brown et al. 2010). Though identified by their location in $\log g - T_{\text{eff}}$ space, few

systems have actually had their radii measured with any precision. Steinfadt et al.’s (2010b) discovery of the eclipsing double WD binary system NLTT 11748 (Kawka & Vennes 2009) allowed for the first geometric measurement of the radius of a ELM WD, finding $R \approx 0.04 R_{\odot}$ for the $0.15 M_{\odot}$ He WD, consistent with the presence of a thick stably-burning hydrogen envelope (also see Kawka, Vennes, & Vaccaro 2010; Kilic et al. 2010a). Additional eclipsing systems (Parsons et al. 2011; Brown et al. 2011b) have led to even more constraints, although for some of the more compact systems it is not clear if the radius is truly the equilibrium radius of the WD or if it has been tidally distorted.

Multiple common envelope phases are possible in the formation scenario for ELM WDs, leading to ELM WDs in binaries with more massive WDs. Many of these will come into contact within 10 Gyr (Figure 1). Indeed, a large number of the known double WD binaries contain ELM WDs ($M_{\text{He}} < 0.20 M_{\odot}$, circled points) with large ($> 0.03 R_{\odot}$) radii indicative of a stable H burning shell (Kawka et al. 2006; Kilic et al. 2007a; Badenes et al. 2009; Mullally et al. 2009; Kilic et al. 2010b; Kulkarni & van Kerkwijk 2010; Marsh et al. 2011; Brown et al. 2011b; Kilic et al. 2011c; Vennes et al. 2011). As noted by D’Antona et al. (2006), since the time to burn the H envelope can easily exceed the time to reach contact, many of these ELM WDs will come into contact with the remaining H envelope. This raises the possibility for many new phenomena that we begin to explore here.

The large radii of the ELM WDs means that Roche lobe overflow (RLO) occurs at larger orbital periods than otherwise expected, so we start in §2 by examining the behavior of the radius of the ELM WD as its H envelope is transferred. We follow in §3 by outlining the basics of mass transfer and highlighting some of the new possibilities when ELM WDs are donors. There is a more distinct possibility for thermally stable burning of the accreted H and He on the accreting WD and the initial contraction of the ELM WD to mass loss allows for more

¹ Physics Department, University of Wisconsin - Milwaukee, Milwaukee WI 53211; kaplan@uwm.edu.

² Kavli Institute for Theoretical Physics and Department of Physics, Kohn Hall, University of California, Santa Barbara, CA 93106; bildsten@kitp.ucsb.edu.

³ Department of Physics, Broida Hall, University of California, Santa Barbara, CA 93106; jdrsteinfadt@gmail.com.

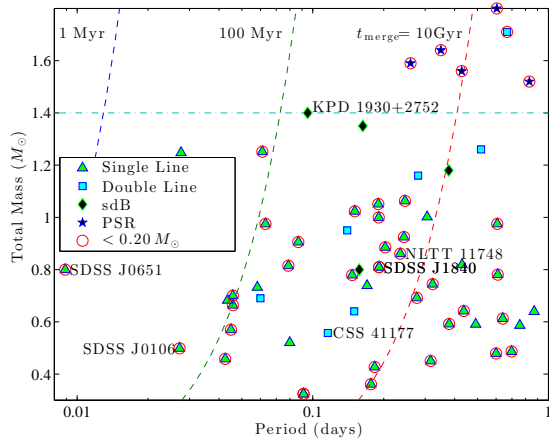


FIG. 1.— The population of double WDs (triangles and squares, depending on whether one or two members of the binary have radial velocity measurements), sdB/WDs (filled diamonds), and pulsar/WDs (filled stars) with $P_{\text{orb}} < \text{day}$. Binaries to the left of the dashed lines will merge in less than 10 Gyr, 100 Myr, or 1 Myr due to gravitational wave losses. Binaries with a ELM He-core WD are circled. Individual sources of interest are labeled: NLTT 11748 (the first eclipsing system), CSS 41177 (the second eclipsing system; Parsons et al. 2011), SDSS J0106–1000 and SDSS J0651+2844 (two recently discovered short period binaries; Kilic et al. 2011c; Brown et al. 2011b), and KPD 1930+2752 (a binary containing a massive WD and a sdB star with a total mass equal to the Chandrasekhar mass; Maxted, Marsh, & North 2000). The line at the Chandrasekhar mass $M_{\text{Ch}} = 1.4 M_{\odot}$ is where a merger could produce a type Ia supernova in the traditional scenario (but see van Kerkwijk, Chang, & Justham 2010). Also see Kilic et al. (2012).

stable mass transfer than that originally found for cold He WDs (Marsh, Nelemans, & Steeghs 2004). We perform the full evolution calculations in §4, highlighting the new phases of H mass transfer, the special behavior near the period minimum, and the likelihood that the intriguing object HM Cancri is one of these systems. We close in §5 by discussing the implications for AM CVn evolution, and the remaining work needed to resolve the thermonuclear outcomes for the accreted matter.

2. ELM STRUCTURE AND RESPONSE TO MASS LOSS

The way in which the donor radius changes with mass loss differentiates the evolution of these ELM donor binaries from the earlier work of Marsh et al. (2004) for cold He WDs, where the WD always becomes larger as mass is removed. This is usually expressed as the logarithmic derivative of radius with respect to mass $\zeta_{\text{He}} \equiv d \ln R_{\text{He}} / d \ln M_{\text{He}}$ which is $\approx -1/3$ for cold, degenerate matter. However, the thick outer layer of non-degenerate and stably-burning hydrogen in an ELM WD dramatically changes ζ_{He} .

For this initial exploration, we use the models of Steinfadt, Bildsten, & Arras (2010a) that provide a range of hydrogen envelope masses M_{env} for each total mass⁴, M_{He} . These represent a large range of ELM

⁴ Some calculations such as Panei et al. (2007) and Althaus, Serenelli, & Benvenuto (2001) find that for masses greater than $\approx 0.2 M_{\odot}$, hydrogen will not burn stably but will instead undergo flashes. However, the precise boundary is not yet known and may be metallicity-dependent. For instance, the recently discovered binary SDSS J065133.33+284423.3 (Brown et al. 2011b) has an ELM WD with a high temperature and a radius indicative of burning even though it is somewhat more massive ($0.25 M_{\odot}$) than the expected burning limit, although for this

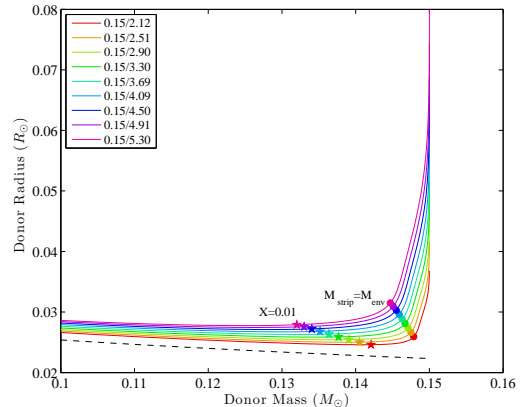


FIG. 2.— Radii of $M_{\text{He}} = 0.15 M_{\odot}$ He WDs as a function of remaining mass as the mass is stripped off. The models are labeled by different starting envelope masses, M_{env} , in units of $10^{-3} M_{\odot}$. We also plot the point where a mass equivalent to the envelope has been stripped (circles) and where the hydrogen mass fraction $X = 0.01$ (stars). Finally, the dashed line is Eggleton’s zero-temperature mass radius relation (Verbunt & Rappaport 1988; Marsh et al. 2004). Because of the diffusive tail, non-zero amounts of hydrogen extend well inward of the point where the stripped mass is equal to the envelope mass.

WD models ($0.125 M_{\odot} \leq M_{\text{He}} \leq 0.20 M_{\odot}$) that adequately cover the possible envelope masses ($M_{\text{env}} = (1 - 5) \times 10^{-3} M_{\odot}$) at the time of Roche lobe contact, or equivalently have ages of 1–13 Gyr; for an age of 1 Gyr, the expected envelope masses according to Panei et al. (2007) are $6 \times 10^{-3} M_{\odot}$ ($M_{\text{He}} = 0.16 M_{\odot}$) to $7 \times 10^{-4} M_{\odot}$ ($M_{\text{He}} = 0.25 M_{\odot}$), but the exact mapping of M_{env} to age is not known in detail. Instead, we verify the starting models by noting that they span the observed range in surface gravity and effective temperature seen in ELM WDs (e.g., Vennes et al. 2011), with $T_{\text{eff}} = 8,000\text{--}20,000\text{ K}$ and $\log(g) = 5 - 7$.

We need to find ζ_{He} as a function of the amount of mass that has been lost, ΔM_{He} , for each distinct initial model. These models have the temperature, pressure and abundance profile of a stably-burning pure H envelope in diffusive equilibrium with the He core. The resulting transitional H/He layer has an abundance profile set by chemical equilibrium in the changing electric field, as described in Steinfadt et al. (2010a). As we show later, the thermal time at the base of the H envelope is longer than the mass transfer timescale, so that the material responds adiabatically to mass loss. To simulate mass loss, we simply go to the mass coordinate $m = M_{\text{tot}} - \Delta M_{\text{He}}$ in the initial model and force that mass element to the surface by making its pressure artificially low (we went to $P = 10^{10} \text{ dyne cm}^{-2}$; in contrast, the pressure at the H/He boundary is $10^{17} \text{ dyne cm}^{-2}$, while the pressure at the core is $> 10^{20} \text{ dyne cm}^{-2}$).

As the underlying fluid elements now have lower pressures, we conserve their entropy by assuming that $TP^{-\gamma}$ is constant, where the adiabatic index γ was $\approx 2/5$ for the region in question. The density is then computed from T and P following the equation-of-state (see Steinfadt et al. 2010a, for details), and the composition of each mass element is assumed to be the same as in

particular object the unknown contribution of tidal heating may contribute to its large size. We limit our exploration to $M_{\text{He}} \leq 0.20 M_{\odot}$.

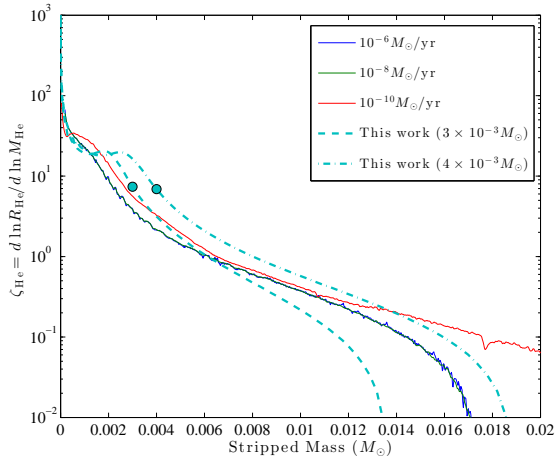


FIG. 3.— Response of the initially stably burning donor to mass stripping $\zeta_{\text{He}} \equiv d \ln R_{\text{He}} / d \ln M_{\text{He}}$ as a function of stripped mass. The initial models were for $M_{\text{He}} = 0.15 M_{\odot}$ He WDs with either a $M_{\text{env}} = 0.003 M_{\odot}$ or $M_{\text{env}} = 0.004 M_{\odot}$ H envelope, undergoing stable hydrogen burning. The dashed/dot-dashed lines show the results of this work using an adiabatic approximation to recalculate the stellar structure, with the filled circles indicating the envelope mass. The solid curves show the dynamical results of MESA (Paxton et al. 2011) for a similar model (albeit with a lower envelope mass of $M_{\text{env}} = 0.0021 M_{\odot}$), using mass-stripping rates of $10^{-6} M_{\odot} \text{ yr}^{-1}$ (blue), $10^{-8} M_{\odot} \text{ yr}^{-1}$ (green), and $10^{-10} M_{\odot} \text{ yr}^{-1}$ (red). Except for the transients at the beginning (which have to do with the outermost layers of the WD) all of the models generally agree for the first 10% of the WD. For the lowest accretion rate (not expected to be adiabatic) the model diverges after $0.015 M_{\odot}$. In all cases, ζ_{He} remains > 1 past twice the envelope mass.

the original model. Therefore, we need only integrate the pressure and radius with respect to the mass coordinate. This integration is done by shooting from the core toward the surface and from the surface toward the core and meeting at a mass coordinate in the middle (the $X = Y$ point, where the hydrogen and helium mass fractions are equal). Selected results for $0.15 M_{\odot}$ ELM WDs are shown in Figure 2, where we plot the radius as a function of the remaining mass along with the zero-temperature (fully degenerate) model used by Marsh et al. (2004). Two things are obvious: (1) as the envelope is stripped, the slope $\zeta_{\text{He}} \gg 1$ so the donor shrinks (as in D’Antona et al. 2006 for stable burners), and the slope is still greater than the $-1/3$ value of the zero-temperature model even once $X < 0.01$; and (2) the radii are always larger than the zero-temperature model, even when the envelope has been stripped, because of the lower initial degeneracy. In our models the larger radii are consequences of both finite ages so that even just passive cooling would result in warmer/larger WDs (unlike in Marsh et al. 2004) and stable H burning (unlike in Deloye et al. 2007). The initial core temperatures at the onset of mass transfer range from 6.7×10^6 K for the $2.1 \times 10^{-3} M_{\odot}$ envelope to 1.4×10^7 K for the $5.3 \times 10^{-3} M_{\odot}$, with higher temperatures resulting in higher initial entropies (Deloye & Bildsten 2003).

In Figure 3 we compare our results for ζ_{He} with those computed using **Modules for Experiments in Stellar Astrophysics** (MESA; Paxton et al. 2011). For our starting points, the models of Steinfadt et al. (2010a) only covered limited values of M_{He} and M_{env} , as we used models that “evolved” from the starting models. Similarly, with MESA we had to use models that we could

construct out of suitable starting conditions, subject to mass loss and diffusive equilibrium. Therefore the comparison is not exact: the MESA model has a total hydrogen mass of $2.1 \times 10^{-3} M_{\odot}$, radius of $0.048 R_{\odot}$, and surface temperature of 7150 K, compared to $(4.0 \times 10^{-3} M_{\odot}, 0.062 R_{\odot}, 7160 \text{ K})$ and $(3.0 \times 10^{-3} M_{\odot}, 0.048 R_{\odot}, 6500 \text{ K})$, for our models. We cannot simultaneously match the envelope mass, radius, and surface temperature. Even so, the agreement for ζ_{He} is good, and the model profiles (the pressure and adiabatic index as functions of radius) agree well. The main apparent difference is the “hump” in ζ_{He} around a stripped mass of $(2-3) \times 10^{-3} M_{\odot}$ visible in our models but not in the MESA models. This occurs slightly before the hydrogen-to-helium transition and near the onset of degeneracy in the original model, and given the different mass coordinates at which this happens in our models versus the MESA models, the discrepancy is not surprising. We see that overall, the shape of ζ_{He} in this adiabatic limit is constant in terms of $\Delta M_{\text{He}} / M_{\text{env}}$.

Whether or not adiabatic evolution is a valid assumption depends on the thermal timescale τ_{th} at the base of the envelope, which is where the luminosity is fixed and most of the excess radius beyond the degenerate helium core is located. Mass-loss will be adiabatic if $M_{\text{env}} / |M| < \tau_{\text{th}}$. For the models of Steinfadt et al. (2010a), τ_{th} is typically a few Myr, so for accretion that is faster than $M_{\text{crit}} \equiv M_{\text{env}} / \tau_{\text{th}} \approx \text{few} \times 10^{-9} M_{\odot} \text{ yr}^{-1}$, our approximation is reasonable, and this regime encompasses most of the evolution we discuss below. For lower mass-loss rates, we should consider thermal evolution during the mass stripping, although at these rates the amount of mass stripped is low enough that it does not significantly affect our results.

3. MASS TRANSFER BASICS

We start with a He WD donor with mass M_{He} that is steadily losing mass onto an accretor (typically a CO WD) with mass M_a . The total mass is $M_t = M_a + M_{\text{He}}$, while the binary orbital separation is a and the orbital angular momentum is $J = M_a M_{\text{He}} (Ga / M_t)^{1/2}$. The mass transfer rate is fixed by the rate of orbital angular momentum loss, \dot{J} via

$$\frac{\dot{J}}{J} = \frac{\dot{M}_a}{M_a} + \frac{\dot{M}_{\text{He}}}{M_{\text{He}}} + \frac{\dot{a}}{2a} - \frac{\dot{M}_t}{2M_t}. \quad (1)$$

The accretor may have intermittent periods of unstable hydrogen burning (classical novae, or CNe) that eject material from the binary; therefore we cannot assume that mass transfer is conservative but must instead track the mass lost by the binary, \dot{M}_t . We write this as $\dot{M}_t = f \dot{M}_{\text{He}}$, so that $f = 1$ means the accretor, on average, keeps a constant mass (e.g., it ejects in each CN the amount of matter that has accreted), and $f = 0$ means that the accretor keeps all the accreted mass. We do not recalculate the accretor’s radius as it gains mass, as this is a small effect for the massive accreting WD. If the CN were to excavate material from the accreting WD, then $f > 1$, although we do not explicitly consider this situation. We write the expression for \dot{J} as

$$\frac{\dot{J}}{J} = \frac{\dot{M}_{\text{He}}}{M_{\text{He}}} \left[1 + (f - 1) \frac{M_{\text{He}}}{M_a} - f \frac{M_{\text{He}}}{2M_t} \right] + \frac{\dot{a}}{2a}, \quad (2)$$

allowing a connection between the mass transfer rate and the loss of orbital angular momentum.

We always assume that the donor’s radius R_{He} tracks that of the Roche lobe, R_L , and use the simple Paczyński (1967) formula for R_L , giving

$$\begin{aligned} \frac{\dot{J}}{J} &= \frac{\dot{M}_{\text{He}}}{M_{\text{He}}} \left[1 + \frac{\zeta_{\text{He}} - \zeta_{r_L}}{2} + (f - 1) \frac{M_{\text{He}}}{M_a} - f \frac{M_{\text{He}}}{2M_t} \right] \\ &\approx \frac{\dot{M}_{\text{He}}}{M_{\text{He}}} \left[\frac{5}{6} + \frac{\zeta_{\text{He}}}{2} + (f - 1) \frac{M_{\text{He}}}{M_a} - f \frac{M_{\text{He}}}{3M_t} \right]. \end{aligned} \quad (3)$$

Here, $\zeta_{r_L} \equiv d \ln r_L / d \ln M_{\text{He}}$ is the derivative of the Roche lobe radius in units of a , $r_L = R_L/a$. The Paczyński approximation is consistent to within about 5% with the results using the Eggleton (1983) formula for r_L for the mass ratios considered here.

At the onset of mass transfer, gravitational-wave losses set \dot{J} to be (Landau & Lifshitz 1975):

$$\frac{\dot{J}_{\text{GR}}}{J} = -\frac{32}{5} \frac{G^3}{c^5} \frac{M_t M_{\text{He}} M_a}{a^4}. \quad (4)$$

This remains true for wide systems, as the material transfers through an accretion disk. However, if there is not enough room for a disk (based on Eqn. 6 of Nelemans et al. 2001) then material will impact directly onto the accretor (Webbink 1984; Marsh et al. 2004). In this case, the angular momentum of the accreted material is lost to the accretor. This angular momentum loss subtracts an additional $\sqrt{r_h(1 + M_{\text{He}}/M_a)}$ from the quantity in the brackets in Eqn. (3), where r_h is the equivalent radius of the material orbiting the accretor (in units of a) as given by Verbunt & Rappaport (1988, correcting for their inverted definition of the mass ratio). In reality, all of the J may not be lost but some may be transferred back to the system via tidal coupling (as in Marsh et al. 2004; Fuller & Lai 2012), but for now we explore the limit where this does not occur since the tidal timescales are largely unconstrained for the accreting WD.

3.1. Burning of the Accreted Material

The importance of knowing the value of f is highlighted by Equation (2). When $f = 0$ (i.e., the transferred material stays on the accretor), the mass ratio M_{He}/M_a decreases even more quickly, reducing dynamical stability (§ 3.2) and increasing $|\dot{M}_{\text{He}}|$. On the other hand, when material is lost from the system (i.e., $f = 1$), then M_{He}/M_a changes more slowly with a corresponding reduction in $|\dot{M}_{\text{He}}|$. It is the ability for the accretor to burn the accreting material at the supplied rate that determines f . Stable burning (i.e., burning the material at the accreted rate in a thermally stable manner) implies $f = 0$, whereas unstable burning results in mass losing events (e.g., classical novae) that drive $f \rightarrow 1$. Since no detailed calculations are available that cover accreted material with our particular abundance mixture (almost pure H going to nearly pure He); we base our current calculations on Papaloizou, Pringle, & MacDonald (1982); Nomoto et al. (2007); Shen & Bildsten (2007) for H burning and Iben & Tutukov (1989) for pure He burning.

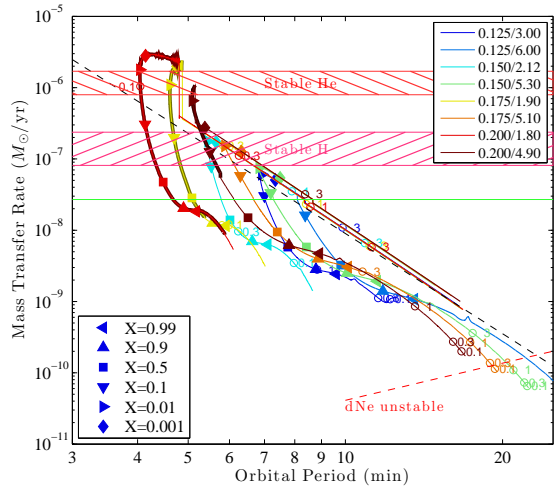


FIG. 4.— Evolution of compact WD binaries involving an ELM He WD and a $0.8 M_{\odot}$ CO WD. The masses of the He WDs vary from $0.125 M_{\odot}$ to $0.2 M_{\odot}$, and the envelope masses (in units of $10^{-3} M_{\odot}$) are also listed. We plot the expected mass-transfer rate \dot{M} from Roche-lobe overflow as a function of orbital period after the systems are brought into contact by GW emission. The systems begin on the lower tracks, move toward shorter orbital periods and increasing \dot{M} , reach a period minimum, and then leave along the upper tracks. The numbers show the ages of the systems (after contact) in Myr. The thick regions are where the accretion stream hits the CO WD directly, instead of forming an accretion disk. The tracks are additionally labeled with symbols that show the hydrogen fraction X of the accreted material, changing from 99% down to 0.1%. The black dashed line is Eqn. 9. The regions where stable H (Nomoto et al. 2007) or He (Iben & Tutukov 1989) burning are possible are shown by the hatched regions, although we use the green horizontal line for the lower H-burning limit to account for reduced metallicity. Finally, the red dashed line shows where accretion is unstable to dwarf novae (dNe) for pure hydrogen, based on Shafter (1992).

The transferred material at the onset of mass transfer is certainly pure hydrogen. If that material does not gain any carbon or oxygen contamination from the accreting WD, then it can only burn via the pp-cycle. Though briefly considered by Papaloizou et al. (1982), no recent calculations have been done to explore the thermal stability of such a pure H layer. Shen & Bildsten (2007) performed stability calculations for very low metallicity, going down to 10^{-4} Solar metallicity. They found that the burning material was more stable, reducing the minimum accretion rate where stable burning can occur by over a factor of three from the limits derived by Nomoto et al. (2007, Eq. 5) for Solar metallicity (shown by the red banded region in Fig. 4). We therefore assume stable hydrogen burning when $\dot{M} > 10^{-7} (M_a/M_{\odot} - 0.5357) M_{\odot} \text{yr}^{-1}$ (the green horizontal line in Fig. 4), and assume that all the accreted mass remains on the accretor ($f = 0$). For rates lower than this, we assume that the H burning is unstable, leading to Roche lobe overflowing nuclear flashes and $f = 1$. However, very little mass is transferred at these low rates, leading to a small impact on the outcome.

The accretion rate needed for stable pure He burning are much higher than those for hydrogen. Just as in H burning, the stability arises due to the increasing importance of radiation pressure and shell thickening, both occurring as the burning luminosity approaches the Eddington limit (Tutukov & Yungelson 1996; Shen & Bildsten 2007). Most thoroughly discussed

in Iben & Tutukov (1989), this rate depends on the WD core mass, and, for the evolution of these binaries, allows for stable He burning only near the period minimum (Tutukov & Yungelson 1996). This results in a narrow range of rates (typically only a factor of ~ 2 , see the hatched region in Fig. 4) for which a WD can stably burn helium. This demands two comparisons for our calculations. First, a tracking of when the accretion rate is in the stable regime and for that duration, a confirmation that enough mass is transferred to build the steady state burning model. Second, when \dot{M} reaches the upper limit of the stable burning regime (meaning that the radius of the accretor exceeds its Roche radius), we must account for the excess transferred matter that cannot be stably burned by the accretor. For this calculation, we simply assume (as is commonly done; Nomoto et al. 2007) that that matter is lost by the binary. Hence, even in the stable regime we will sometimes set f to a value that is different than zero.⁵ We do this so that $|\dot{M}_{\text{He}}|$ does not exceed the limit for stable He burning (essentially the Eddington limit). When these conditions occur in our evolutionary scenarios, its almost always the case that $X \approx 0$. Eventually, as the orbit widens, $|\dot{M}_{\text{He}}|$ decreases below the lower limit for stable He burning, and we set $f = 1$ again.

3.2. Enhanced Stability of Mass Transfer from an ELM

Mass transfer is dynamically stable when the term in the brackets in Eqn. (3) is positive for $f = 0$. If it is negative, the stellar radius will be larger than the Roche radius after mass transfer, leading to a dynamical instability and merger. The form of this condition depends on whether the angular momentum of the material which leaves the donor can get back into the orbital angular momentum (as assumed in disk accretion) or becomes “lost” in the accretor during direct impact. Accretion via a disk is stable when

$$\frac{M_{\text{He}}}{M_a} < \frac{5}{6} + \frac{\zeta_{\text{He}}}{2}. \quad (5)$$

For a cold WD, $R_{\text{He}} \propto M_{\text{He}}^{-1/3}$, leading to $\zeta_{\text{He}} = -1/3$. This would imply stability if $M_{\text{He}}/M_a < 2/3$, the traditional criterion for stability. The additional angular momentum loss allowed by direct-impact changes the criterion to:

$$\frac{M_{\text{He}}}{M_a} < \frac{5}{6} + \frac{\zeta_{\text{He}}}{2} - \sqrt{\left(1 + \frac{M_{\text{He}}}{M_a}\right) r_h}. \quad (6)$$

This substantially reduces the allowed mass ratios for initially stable mass transfer (Marsh et al. 2004) especially for cold WDs, or those with a finite entropy (Deloye et al. 2007) but no burning.

However, as we show in Figure 3, He WDs with thick, massive hydrogen layers have $\zeta_{\text{He}} \gg 1$ for stripped masses $\Delta M_{\text{He}}/M_{\text{He}} \lesssim 10\%$. D’Antona et al. (2006) were the first to explore the possibly different evolutions this

⁵ In contrast to the majority of our numerical integrations where we use an adaptive step size 4th/5th-order Runge-Kutta integrator, updating the value of f is done so as to keep the rate of accreted material for the last iteration in the stable regime — no higher order derivative is used — which leads to the apparent numerical noise in Figure 4. This does not affect the outcome.

allows for. Just from Eqn. (5), $M_{\text{He}} < M_a$ mass transfer will be dynamically stable as long as there is an accretion disk. Even without a disk (using Eqn. 6), the additional term $\sqrt{(1 + M_{\text{He}}/M_a)r_h}$ is roughly ≈ 0.5 , so as long as ζ_{He} is positive we still have dynamical stability. Hence, for almost all the mass ratios considered here, dynamical instability is not possible for disk-fed accretion and could only happen for direct-impact accretion when $M_{\text{He}}/M_a \gtrsim 1/4$ (assuming a typical $\zeta_{\text{He}} = -1/3$ once the hydrogen envelope has been fully stripped). Tidal interactions could work to stabilize these few unstable mass transfer cases (as in Marsh et al. 2004), but that is beyond the scope of our work.

4. EVOLUTION INCLUDING MASS TRANSFER FROM AN ELM WD

Just as in the conventional double WD binaries, the lower mass ELM WD will be driven into contact by the loss of angular momentum from gravitational waves. For the more massive companion, we presume cold CO WDs with masses $0.7\text{--}1.0 M_{\odot}$ (we do not discuss masses $< 0.7 M_{\odot}$, as those are not covered by the calculations of Nomoto et al. 2007). We neglect any tidal heating of the ELM WD prior to contact, and simply assume, as in the previous section, that it has a thick H envelope that is stably burning. We start by discussing the long period of stable mass transfer of the overlying H shell, then discuss the behavior near the period minimum and close with a brief discussion of the outgoing He mass transfer phase; which is similar to that previously discussed in the literature.

4.1. Mass Transfer Phase up to the Period Minimum

The larger stellar radius leads to the onset of mass transfer at orbital periods of ~ 10 minutes, much longer than expected for a thin-H-shell cooling WD. Since $\zeta_{\text{He}} \gg 1$, the donor shrinks under mass loss, so the mass transfer is stable and secularly driven at the rate implied by equation (3) when angular momentum loss is fixed by gravitational radiation (see Eqn. 4). We explore a range of ELM WDs with masses $M_{\text{He}}/M_{\odot} = 0.125\text{--}0.20$ and envelopes of $M_{\text{env}} = 1.5 \times 10^{-3}$ to $5.1 \times 10^{-3} M_{\odot}$, although a single donor mass only has part of the range. Not all of these are physically realistic: some higher-mass WDs may not have stable burning, or some combinations of envelope and total mass may not be reachable in a Hubble time (see discussions in Panei et al. 2007 and Steinfadt et al. 2010a).

We start our calculation when mass transfer begins (also see D’Antona et al. 2006), typically at orbital periods of 6–10 minutes. Figure 5 shows the resulting evolution up to the period minimum for two cases with $M_{\text{He}} = 0.15 M_{\odot}$ and $0.2 M_{\odot}$. For these cases, the accretion rate, \dot{M} , is in the range where our adiabatic approximation is valid.⁶ The increase in $|\dot{M}|$ as the orbital period shrinks is evident. At the earliest part of the onset of accretion, the orbital \dot{P} (second panel) is nearly identical to that calculated (dot-dashed lines in the second panel) from the loss of angular momentum

⁶ Other cases we show in a Figure 4 that come into contact at much wider orbital periods violate this inequality, but in those cases the amount of mass transferred at this low rate is small enough as to not qualitatively change the results.

from two orbiting point masses. Namely, if measured at this stage, the system would appear to have an orbital period change consistent with gravitational inspiral (D’Antona et al. 2006, also see Fig. 6). During this initial evolution we have $\zeta_{\text{He}} \gg \zeta_{rL}$, and we find from Eqns. (3) and (4) that

$$|\dot{M}_{\text{He}}|_{\text{in}} \approx \frac{64M_{\text{He}}^2 M_a}{5c^5 \zeta_{\text{He}}} \left(\frac{256\pi^8 G^5}{M_t P^8} \right)^{1/3}, \quad (7)$$

highlighting the need to calculate the considerable evolution in ζ_{He} during this period (Fig. 5) to find \dot{M}_{He} .

This evolution is a new mode of H mass transfer onto a WD that has not been previously explored over a wide range of initial masses with semi-analytic models. The long (\sim Gyr) life of the ELM WD prior to contact has allowed for complete diffusive equilibrium so that the transferred material is pure hydrogen at the start, with an increasing amount of helium at later times as the stripping reveals the underlying He WD core (5th panel in Figure 5). The amount of mass that has been stripped (third panel down) is simply what’s needed to keep the stellar radius equal to the Roche radius as the donor moves inward. These are often but not always disk accretors but compact enough that the thermal disk instability that gives rise to dwarf novae is suppressed (systems below the dashed line on Figures 4 and 7 would undergo dwarf novae instabilities).

The thermonuclear outcomes during this phase remain uncertain until a time dependent accretion calculation has been performed with the changing \dot{M} and X of Figure 5. However, as we discussed in § 3.1, if H mass transfer leads to stable burning, the system’s luminosity would increase to $L = Q_{\text{nuc}} \dot{M}$.

4.2. Near the Period Minimum and The Ultra-Compact Binary HM Cnc

After the initial evolution the degenerate portions of the donor come to the surface and a minimum period is reached. This minimum is near where $|\dot{M}|$ is maximum, where direct impact often starts (forcing us to adjust \dot{J} accordingly), and where the mass transfer can in principle become dynamically unstable. For less massive accretors direct-impact accretion will always happen. The mass-transfer rate is shown in Figures 4 and 7 for a single accretor mass and a range of donor masses, while Figure 6 shows the orbital period derivative. The mass-transfer factor f is calculated according to § 3.1.

The interacting binary star HM Cancri (HM Cnc or RXJ0806.3+1527) has an orbital period of 5.4 min (Israel et al. 1999; Ramsay, Hakala, & Cropper 2002; Israel et al. 2002). Spectroscopy (Roelofs et al. 2010) supports a model with two interacting white dwarfs consistent with masses of $0.27 M_{\odot}$ and $0.55 M_{\odot}$ but with the actual values unconstrained. X-ray observations show a decreasing orbital period (Strohmayer 2005) at a rate consistent with gravitational-wave emission, as shown in Figure 6 (where we highlight it’s value of P and \dot{P}). While the X-ray luminosity was puzzlingly low for accretion from a degenerate companion, D’Antona et al. (2006) showed that the implied transfer rate was much more consistent with an ELM WD donor. We find the same conclusion, which is that HM Cnc is consistent

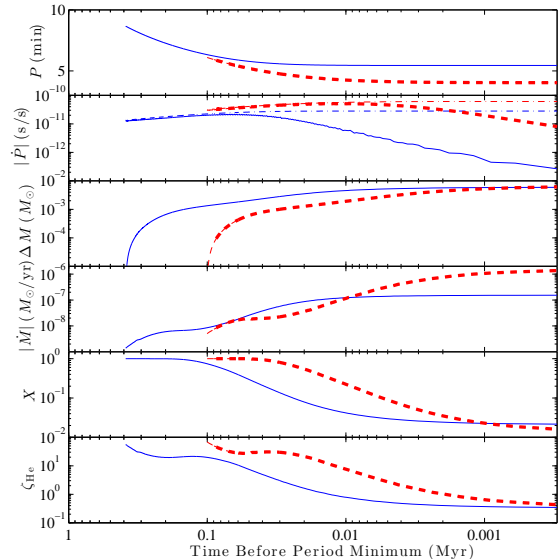


FIG. 5.— Evolution of compact WD binaries involving an ELM He WD and a $M_a = 0.8M_{\odot}$ CO WD. The masses of the He WDs are $M_{\text{He}} = 0.15M_{\odot}$ (blue solid line) and $M_{\text{He}} = 0.2M_{\odot}$ (red dashed line), with envelope masses of $M_{\text{env}} = 2.1 \times 10^{-3} M_{\odot}$ and $M_{\text{env}} = 1.8 \times 10^{-3} M_{\odot}$, respectively. We plot (top to bottom) the orbital period, the orbital period derivative, the transferred mass, the accretion rate, the hydrogen mass fraction, and ζ_{He} . The period of direct-impact accretion for the $M_{\text{He}} = 0.2M_{\odot}$ WD is indicated by the thick dashed line. In the \dot{P} panel, the red and blue dot-dashed lines are where the loss of angular momentum is entirely given by Eqn. (4).

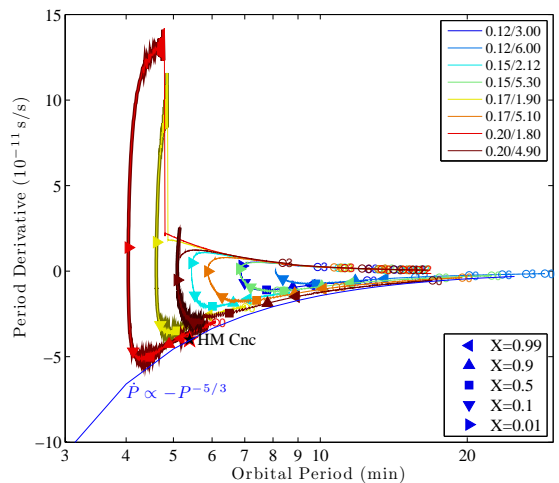


FIG. 6.— Period derivative vs. orbital period for a compact WD binaries involving an ELM He WD and a $0.8M_{\odot}$ CO WD. The different donor models are as in Figure 4. We also show the expected $\dot{P} \propto -P^{-5/3}$ behavior along the incoming (lower) track (Eqn. 10) as expected from gravitational inspiral. We also show the observed properties of HM Cnc.

with accretion from an ELM WD that is still inspiraling and transferring H-rich material. Such a system, along with other short-period binaries like V407 Vul (RX J1914.4+2456; Cropper et al. 1998), are extremely valuable as probes of the eventual fates of systems like those in Figure 1.

4.3. Impact on AM CVn formation

Differentiating between the different possible outcomes based on the progenitors characteristics is a major goal of work like that described here. In particular, we seek to separate the systems that will remain separate from those that will merge. Systems that remain stable will move to longer orbital periods with declining accretion rates and become AM CVn binaries: systems that have a prolonged period of He mass transfer driven by gravitational wave emission. In contrast, those that become unstable will shred the He WD into a rapidly rotating hot disk that likely becomes an R CrB star (Saio & Jeffery 2002). Marsh et al. (2004) did this in detail by considering the stability of mass transfer, including the unknown effects of tidal coupling.

Based on the qualitative effects described in § 3.2, we can examine here whether more systems will remain stable. This will directly influence population calculations (e.g., Brown et al. 2011a), which find only a small fraction of the total AM CVn population could come from ELM WD binaries, although based on the limited parameter space that we explore we do not make population predictions in this work.

In Figure 8 we differentiate between those systems that has disk-fed accretion and those that undergo direct impact. For all of the systems that we study dynamical stability (Eqns. 5 or 6) is maintained. We also see that the increased size and decreased degeneracy of the donor which begins mass transfer at larger separations means that more space is available for accretion disks. The exact threshold depends on both the donor’s core and envelope masses, although in general it increases by about $0.03 M_{\odot}$ or so compared to the threshold for a cold donor in Marsh et al. (2004).

While none of the systems we study is dynamically unstable, this is largely because we do not include the less massive accretors ($0.4\text{--}0.6 M_{\odot}$) which appear common (Kilic et al. 2012) and which would be closer to the stability threshold. Extending our calculation to lower accretor masses with the addition of improved stable-burning thresholds will help investigate dynamical stability more closely, but the qualitative behavior of an increased range of systems maintaining accretion disks and remaining stable will hold. Current estimates, based on rather small samples of ELM WDs and AM CVns, suggest that only a small fraction of AM CVns come from ELM WDs (Brown et al. 2011a), but significant improvements in the AM CVn population (e.g., Levitan et al. 2011) and evolutionary calculations may change this conclusion. It is clear that this increased phase space for stable accretion outcomes demonstrated here will lead to a higher yield of AM CVn binaries from double WDs.

4.4. Stable Outgoing Helium Transfer

The final behavior is familiar and the change in J is determined not by the change in a but by the mass transferred. The mass-radius relation of the donor determines the evolution. In this range, ζ_{He} is roughly constant (the classical value is $-1/3$, and in our model is it close to $-1/4$). With that, we find

$$P \approx \frac{9\pi}{\sqrt{2G}} \left[R_0 \left(\frac{M_{\text{He}}}{M_0} \right)^{\zeta_0} M_{\text{He}}^{-1/3} \right]^{3/2} \quad (8)$$

where $R_{\text{He}} = R_0(M_{\text{He}}/M_0)^{\zeta_0}$, and ζ_0 is the final constant value of ζ_{He} . With this, we ignore the terms in the brackets in Eqn. (2) that contain M_{He} since they are less than the other terms ($5/6 + \zeta_{\text{He}}/2$), and find:

$$|\dot{M}_{\text{He}}|_{\text{out}} \approx \frac{7776 M_0 M_a R_0^3}{5 c^5} \left(\frac{4\pi^{14} G^2}{M_t P^{14}} \right)^{1/3} \quad (9)$$

in the limit that $\zeta_0 \approx -1/3$. With $\zeta_0 = -1/4$, the exponent on P changes from $-14/3 = 4.67$ to $-104/21 = 4.95$.

Based on these, we can determine \dot{P} along the incoming and outgoing branches:

$$\begin{aligned} \dot{P}_{\text{in}} &= \frac{-384 M_{\text{He}}}{5 c^5} \left(\frac{4\pi^8 G^5 M_a^2}{P^5} \right)^{1/3} \\ \dot{P}_{\text{out}} &= \frac{1728}{5 c^5} \left(\frac{2\pi^{22} G^7 R_0^9 M_0^3 M_a^4}{P^{16}} \right)^{1/6} \end{aligned} \quad (10)$$

This then allows us to determine the relative populations of objects along the incoming and outgoing branches. This is just the ratio of the \dot{P} ’s, since the time spent ($\propto 1/\dot{P}$) is related to the population:

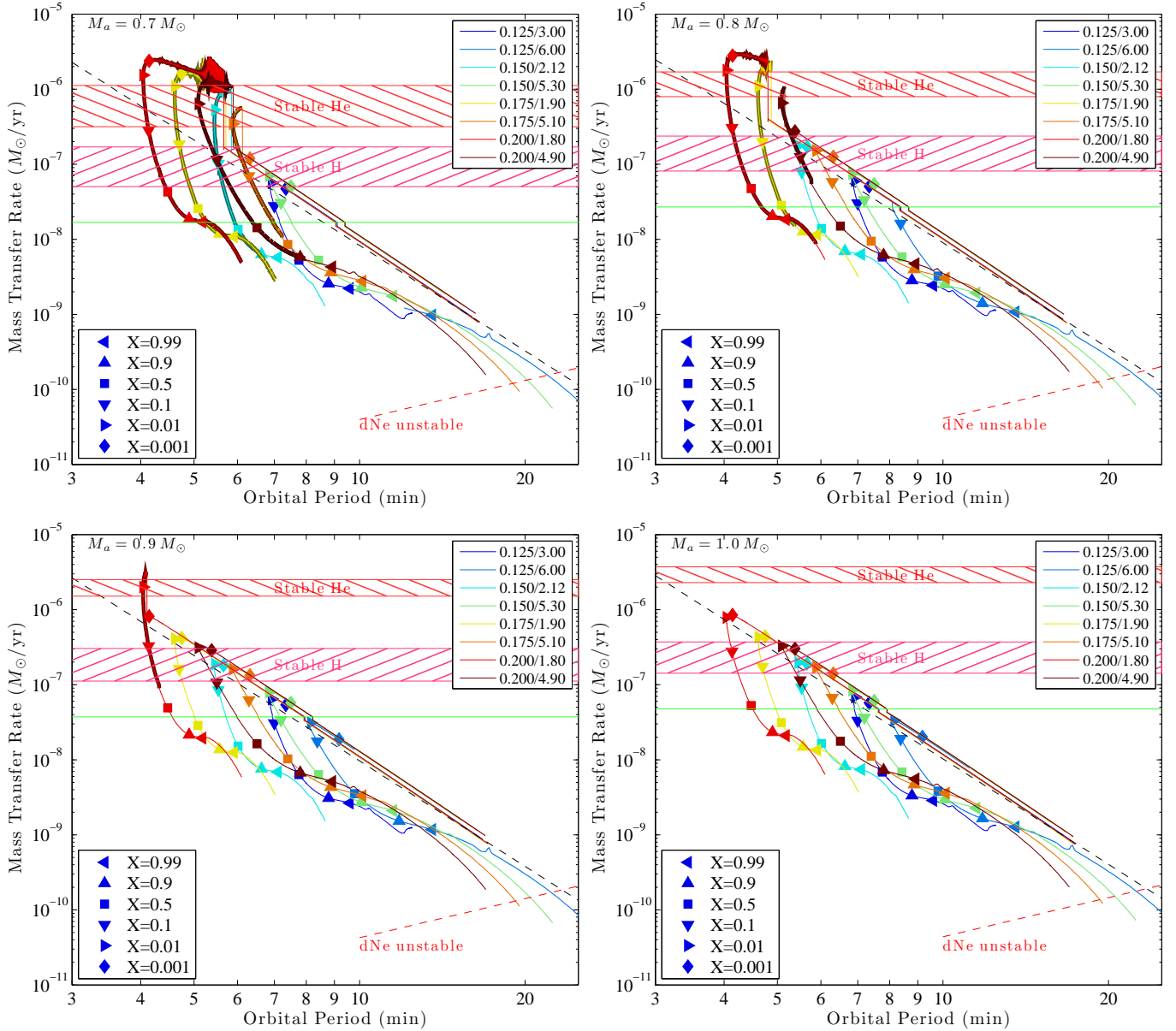
$$\mathcal{N}_{\text{out/in}} \equiv \left| \frac{\dot{P}_{\text{in}}}{\dot{P}_{\text{out}}} \right| \approx \sqrt{\frac{8G}{M_0}} \frac{P M_{\text{He}}}{9\pi R_0^{3/2}}. \quad (11)$$

Based on our model, $R_0 = 0.034 R_{\odot}$ at $M_0 = 0.05 M_{\odot}$, so $\mathcal{N}_{\text{out/in}} \approx 4(P/10 \text{ min})(M_{\text{He}}/0.15 M_{\odot})$ where the mass of the He WD is the original mass along the incoming track. This shows that if every AM CVn had an ELM WD as the originating double WD binary, then there is one inspiraling H mass transferring system for every 4 AM CVns at an orbital period of 10 minutes. Note that this is not true in the period/mass range where direct-impact accretion occurs (as presumably for HM Cnc), as that dramatically increases $|\dot{P}_{\text{out}}|$ and so reduces the outgoing (AM CVn) population. In any case, finding these predicted systems remains a challenge.

D’Antona et al. (2006) found it unlikely that V407 Vul had the same origin as HM Cnc, as the lifetimes on the incoming versus outgoing branches would suggest that its orbital period should be increasing rather than decreasing (Strohmayer 2002 find $\dot{P} = -2.6 \times 10^{-12} \text{ s s}^{-1}$ at an orbital period of 9.5 min). We do not find quite such a strong preference, with $\mathcal{N}_{\text{out/in}} \approx 2\text{--}4$ depending on the accretor mass (compared to a ratio of about 5 in D’Antona et al. 2006). Still, the small orbital period derivative of V407 Vul is somewhat difficult to explain, being a factor of 2 smaller than the lowest value we find in Figure 6. Considering lower accretor masses may help resolve this.

5. CONCLUSIONS

We have shown that the unique properties of ELM WDs — large, nondegenerate H-rich shells supported by stable H burning — lead to some new phenomena when mass transfer initiates in double-WD binaries. There is a prolonged period of H-rich mass transfer at a low rate during inspiral, with HM Cnc potentially being the prototype. The change in the mass-radius relation for the donor creates an intrinsically more stable binary



that opens up additional phase space for making stable He accreting binaries. ELMs will increase the AM CVn birthrate, potentially alleviating the apparent paucity of progenitor systems. Those AM CVns which emerged from this progenitor scenario will also have a larger He core radius than expected from an initially cold WD, thereby exhibiting a higher accretion rate at a fixed orbital period than from a cold WD (Deloye & Bildsten 2003).

Prior to the onset of mass transfer, the ELM WDs had Gyrs to undergo diffusive settling and substantial burning of hydrogen. That clearly allows for the complete sedimentation of the heavier elements from the outermost layers of the WD. Hence, the mass transferred will vary from nearly pure H, to nearly pure He. As we discussed, much work remains to more carefully calculate

the thermodynamic outcomes from this mass transfer. If more thermally stable, then these systems may become more observationally detectable due to the higher luminosities. It is also interesting to note the pronounced absence of heavy elements in the x-ray spectra of HM Cnc (Strohmayer 2008), also pointing to an ELM origin that lived a long time prior to mass transfer initiation. If thermally unstable, then the accumulated mass could ignite explosively (Bildsten et al. 2007), potentially contributing to the increasing number of low-luminosity ‘‘supernovae’’ observed locally (e.g., Kasliwal et al. 2010).

We thank Bill Paxton for advice on running MESA, and thank Bill Paxton and Ken Shen for helpful discussions. This research has been supported by the National Science Foundation under grants PHY 11-25915 and AST 11-09174.

REFERENCES

Althaus, L. G., Serenelli, A. M., & Benvenuto, O. G. 2001, MNRAS, 323, 471

Badenes, C., Mullally, F., Thompson, S. E., & Lupton, R. H. 2009, ApJ, 707, 971

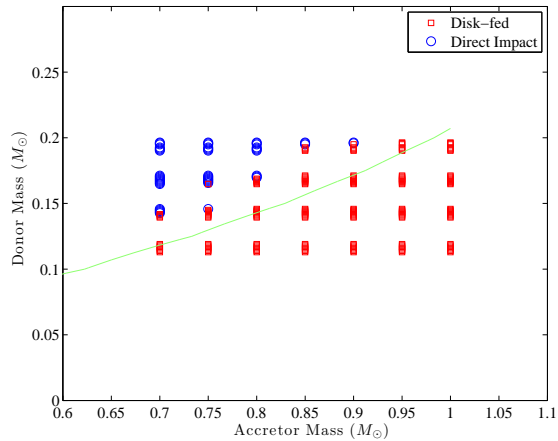


FIG. 8.— Stability of mass transfer for different values of the donor and accretor mass, following Marsh et al. (2004, Fig. 1). For each of our model calculations (some of which are shown in Fig. 7), we plot a square if the accretion is always disk-fed (and hence guaranteed stable) and a circle if it enters a direct-impact period. For each combination of donor and accretor mass, the different models correspond to different envelope masses that have been slightly offset vertically, for clarity. The diagonal line is the direct/disk line from Marsh et al. (2004), using their cold equation-of-state for the donor.

- Bassa, C. G., van Kerkwijk, M. H., Koester, D., & Verbunt, F. 2006, *A&A*, 456, 295
- Bildsten, L., Shen, K. J., Weinberg, N. N., & Nelemans, G. 2007, *ApJ*, 662, L95
- Brown, W. R., Kilic, M., Allende Prieto, C., & Kenyon, S. J. 2010, *ApJ*, 723, 1072
- . 2011a, *MNRAS*, 411, L31
- Brown, W. R., Kilic, M., Hermes, J. J., Allende Prieto, C., Kenyon, S. J., & Winget, D. E. 2011b, *ApJ*, 737, L23
- Cropper, M., Harrop-Allin, M. K., Mason, K. O., Mittaz, J. P. D., Potter, S. B., & Ramsay, G. 1998, *MNRAS*, 293, L57
- D'Antona, F., Ventura, P., Burderi, L., & Teodorescu, A. 2006, *ApJ*, 653, 1429
- D'Cruz, N. L., Dorman, B., Rood, R. T., & O'Connell, R. W. 1996, *ApJ*, 466, 359
- Deloye, C. J. & Bildsten, L. 2003, *ApJ*, 598, 1217
- Deloye, C. J., Taam, R. E., Winisdoerffer, C., & Chabrier, G. 2007, *MNRAS*, 381, 525
- Eggleton, P. P. 1983, *ApJ*, 268, 368
- Eisenstein, D. J., et al. 2006, *ApJS*, 167, 40
- Fuller, J. & Lai, D. 2012, *MNRAS*, 421, 426
- Hansen, B. M. S. 2005, *ApJ*, 635, 522
- Iben, Jr., I. & Livio, M. 1993, *PASP*, 105, 1373
- Iben, Jr., I. & Tutukov, A. V. 1989, *ApJ*, 342, 430
- Israel, G. L., et al. 2002, *A&A*, 386, L13
- Israel, G. L., Panzera, M. R., Campana, S., Lazzati, D., Covino, S., Tagliaferri, G., & Stella, L. 1999, *A&A*, 349, L1
- Kalirai, J. S., Bergeron, P., Hansen, B. M. S., Kelson, D. D., Reitzel, D. B., Rich, R. M., & Richer, H. B. 2007, *ApJ*, 671, 748
- Kasliwal, M. M., et al. 2010, *ApJ*, 723, L98
- Kawka, A. & Vennes, S. 2009, *A&A*, 506, L25
- Kawka, A., Vennes, S., Oswalt, T. D., Smith, J. A., & Silvestri, N. M. 2006, *ApJ*, 643, L123
- Kawka, A., Vennes, S., & Vaccaro, T. R. 2010, *A&A*, 516, L7
- Kilic, M., Allende Prieto, C., Brown, W. R., Agüeros, M. A., Kenyon, S. J., & Camilo, F. 2010a, *ApJ*, 721, L158
- Kilic, M., Brown, W. R., Allende Prieto, C., Agüeros, M. A., Heinke, C., & Kenyon, S. J. 2011a, *ApJ*, 727, 3
- Kilic, M., Brown, W. R., Allende Prieto, C., Kenyon, S. J., Heinke, C. O., Agüeros, M. A., & Kleinman, S. J. 2012, *ApJ*, 751, 141
- Kilic, M., Brown, W. R., Allende Prieto, C., Kenyon, S. J., & Panei, J. A. 2010b, *ApJ*, 716, 122
- Kilic, M., Brown, W. R., Allende Prieto, C., Pinsonneault, M. H., & Kenyon, S. J. 2007a, *ApJ*, 664, 1088
- Kilic, M., Brown, W. R., Hermes, J. J., Allende Prieto, C., Kenyon, S. J., Winget, D. E., & Winget, K. I. 2011b, *MNRAS*, 418, L157
- Kilic, M., et al. 2011c, *MNRAS*, 413, L101
- Kilic, M., Stanek, K. Z., & Pinsonneault, M. H. 2007b, *ApJ*, 671, 761
- Kulkarni, S. R. & van Kerkwijk, M. H. 2010, *ApJ*, 719, 1123
- Landau, L. D. & Lifshitz, E. M. 1975, *The classical theory of fields*, 4th edn. (Oxford, UK: Pergamon Press)
- Levitani, D., et al. 2011, *ApJ*, 739, 68
- Marsh, T. R. 2011, *Classical and Quantum Gravity*, 28, 094019
- Marsh, T. R., Dhillon, V. S., & Duck, S. R. 1995, *MNRAS*, 275, 828
- Marsh, T. R., Gänsicke, B. T., Steeghs, D., Southworth, J., Koester, D., Harris, V., & Merry, L. 2011, *ApJ*, 736, 95
- Marsh, T. R., Nelemans, G., & Steeghs, D. 2004, *MNRAS*, 350, 113
- Maxted, P. F. L., Marsh, T. R., & North, R. C. 2000, *MNRAS*, 317, L41
- Mullally, F., Badenes, C., Thompson, S. E., & Lupton, R. 2009, *ApJ*, 707, L51
- Nelemans, G., Portegies Zwart, S. F., Verbunt, F., & Yungelson, L. R. 2001, *A&A*, 368, 939
- Nomoto, K., Saio, H., Kato, M., & Hachisu, I. 2007, *ApJ*, 663, 1269
- Paczynski, B. 1967, *Acta Astron.*, 17, 287
- Panei, J. A., Althaus, L. G., Chen, X., & Han, Z. 2007, *MNRAS*, 382, 779
- Papaloizou, J. C. B., Pringle, J. E., & MacDonald, J. 1982, *MNRAS*, 198, 215
- Parsons, S. G., Marsh, T. R., Gänsicke, B. T., Drake, A. J., & Koester, D. 2011, *ApJ*, 735, L30
- Paxton, B., Bildsten, L., Dotter, A., Herwig, F., Lesaffre, P., & Timmes, F. 2011, *ApJS*, 192, 3
- Ramsay, G., Hakala, P., & Cropper, M. 2002, *MNRAS*, 332, L7
- Roelofs, G. H. A., Rau, A., Marsh, T. R., Steeghs, D., Groot, P. J., & Nelemans, G. 2010, *ApJ*, 711, L138
- Saio, H. & Jeffery, C. S. 2002, *MNRAS*, 333, 121
- Serenelli, A. M., Althaus, L. G., Rohrmann, R. D., & Benvenuto, O. G. 2002, *MNRAS*, 337, 1091
- Shafter, A. W. 1992, *ApJ*, 394, 268
- Shen, K. J. & Bildsten, L. 2007, *ApJ*, 660, 1444
- Steinfadt, J. D. R., Bildsten, L., & Arras, P. 2010a, *ApJ*, 718, 441
- Steinfadt, J. D. R., Kaplan, D. L., Shporer, A., Bildsten, L., & Howell, S. B. 2010b, *ApJ*, 716, L146
- Strohmayer, T. E. 2002, *ApJ*, 581, 577
- Strohmayer, T. E. 2005, *ApJ*, 627, 920
- . 2008, *ApJ*, 679, L109
- Tutukov, A. & Yungelson, L. 1996, *MNRAS*, 280, 1035
- van Kerkwijk, M. H., Bergeron, P., & Kulkarni, S. R. 1996, *ApJ*, 467, L89
- van Kerkwijk, M. H., Chang, P., & Justham, S. 2010, *ApJ*, 722, L157
- Vennes, S., et al. 2011, *ApJ*, 737, L16
- Verbunt, F. & Rappaport, S. 1988, *ApJ*, 332, 193
- Webbink, R. F. 1984, *ApJ*, 277, 355